IEEE Access
Multidisciplinary | Rapid Review | Open Access Journal

Received January 29, 2019, accepted February 13, 2019, date of publication February 21, 2019, date of current version March 12, 2019.

*Digital Object Identifier 10.1109/ACCESS.2019.2900712*

# Discrete Interference Suppression Method Based on Robust Sparse Bayesian Learning for STAP

**XIAOPENG YANG[1,2], (Senior Member, IEEE), YUZE SUN[3], JIAN YANG[3], (Senior Member, IEEE), TENG LONG[1,2], (Fellow, IEEE), AND TAPAN K. SARKAR[4], (Fellow, IEEE)**

[1]School of Information and Electronics, Beijing Institute of Technology, Beijing 100081, China
[2]Key Laboratory of Electronic and Information Technology in Satellite Navigation (Beijing Institute of Technology), Ministry of Education, Beijing 100081, China
[3]Department of Electronic Engineering, Tsinghua University, Beijing 100084, China
[4]Department of Electrical Engineering and Computer Science, Syracuse University, Syracuse, NY 13244, USA

Corresponding author: Xiaopeng Yang (xiaopengyang@bit.edu.cn)

This work was supported in part by the National Natural Science Foundation of China under Grant 61490693, Grant 61860206012, Grant 61671065, and Grant 31727901 and the 111 Project of China under Grant B14010.

**ABSTRACT** Discrete interference influences the performance of existing space-time adaptive processing methods in practical scenarios. In order to effectively suppress discrete interference in real clutter environment, a discrete interference suppression method based on robust sparse Bayesian learning (SBL) is proposed for airborne phased array radar. In the proposed method, the estimation of spatial-temporal spectrum and the calibration of space-time overcomplete dictionary are carried out iteratively. During one iteration, the prominent components of clutter and discrete interference in the spatial-temporal plane are first estimated by SBL, and then the overcomplete dictionary is calibrated by calculating the error matrix. Because of the robust estimation of spatial-temporal spectral distribution, both the discrete interference and the homogeneous clutter profiles can be effectively suppressed with a small number of space-time data. The effectiveness of the proposed method is verified in the nonhomogeneous environment by utilizing simulated and actual airborne phased array radar data.

**INDEX TERMS** Discrete interference suppression, nonhomogeneous clutter, sparse Bayesian learning (SBL), STAP.

## I. INTRODUCTION

Space-time adaptive processing (STAP) is considered as an effective clutter suppression technique for advanced airborne phased array radar [1], [2]. Based on the adaptive filtering in the spatial-temporal domain, the STAP methods can provide more effective detection performance of low-velocity targets in clutter than traditional non-adaptive methods. However, it is well known that conventional STAP methods need a larger amount of independent and identically distributed (i.i.d.) training data around the tested range cell for estimating the clutter covariance matrix, thus the applicability of the STAP technique is heavily limited in many real nonhomogeneous clutter environments, where high towers, high-speed vehicles and other locally distributed clutter are probably located in the tested range cell rather than the surrounding range cells. Therefore, conventional STAP cannot form adaptive nulls in the directions of such discrete interference. In this case, great performance loss would occur for STAP methods [4], [5]. Therefore it is critical to investigate effective discrete interference suppression methods.

Aiming at this problem, several methods have been proposed for the discrete interference suppression [4]–[7]. It is known that the direct data domain (DDD) method can adaptively suppress the discrete interference while achieving the target detection [4], [5]. However, as it only utilizes the tested range cell data, the statistical property of the homogeneous clutter is ignored, so the homogeneous clutter cannot be suppressed effectively by the DDD method. Later the hybrid space-time methods based on adaptive local transformation were proposed for discrete interference suppression [6]–[8]. By forming the adaptive local transformation matrix with

The associate editor coordinating the review of this manuscript and approving it for publication was Ahmet M. Elbir.

a series of DDD weight vector to take the advantage of statistical STAP and DDD method, the hybrid method suppresses both the discrete interference and homogeneous clutter. However, it is still hard to collect sufficient i.i.d. space-time training data in the practical environment, so the performance of this hybrid method would be severely degraded due to the inferior clutter estimation.

In the last few decades, by developing the sparse property of the clutter in the spatial-temporal domain, several sparsity-based STAP methods were proposed to realize the estimation of the spatial-temporal clutter spectrum with much less training space-time data [9]–[12]. In these methods, the sparse recovery of spatial-temporal clutter spectrum is usually formulated as a regularized optimization problem [11]. However the computational complexity will increase rapidly when the dimension of optimization problem increases, making it unrealizable for application. Afterwards many fast sparse recovery methods were later proposed for STAP in [13]–[17]. One is the FOCal Underdetermined System Solution (FOCUSS), which uses the weighted $L_2$-norm minimization to recursively achieve an approximate estimation of the prominent clutter and discrete interference profiles [13]. However, because the performance is heavily influenced by the overcomplete dictionary mismatch and the regularization parameter cannot be adjusted adaptively, the performance of FOCUSS would degrade in practical application.

In recent years, the Sparse Bayesian learning (SBL) is used in many areas, such as direction of arrival (DOA) estimation [19], [20], microwave imaging [20], [21], linear array synthesis [22] and STAP [17], [23], [24]. Some SBL methods are developed based on the maximum a posteriori (MAP) principle [25]–[27], which optimizes a multi-variable objective function by maximizing the joint probability density function (PDF). On the other hand, some other SBL methods are based on the relevance vector machine (RVM) principle, which achieves the optimization with the help of relevant hyper-parameter [28], [29]. Although the SBL methods of RVM principle can obtain desirable reconstruction performance, the computation of hyper-parameters is extremely complicated, leading to a high computational complexity for sparse recovery.

In this paper, a discrete interference suppression method is proposed for STAP, which is based on robust SBL with the MAP principle. In the proposed method, the estimation of spatial-temporal spectrum and the calibration of space-time overcomplete dictionary are carried out iteratively. During one iteration, the prominent components of clutter and discrete interference in the spatial-temporal plane are firstly estimated by SBL, and then the overcomplete dictionary is calibrated by calculating the error matrix. Because of the robust estimation of spatial-temporal spectral distribution, both the discrete interference and the homogeneous clutter profiles can be effectively suppressed with a small number of space-time data. The proposed method improves the performance at a low computational cost compared with existing STAP methods.

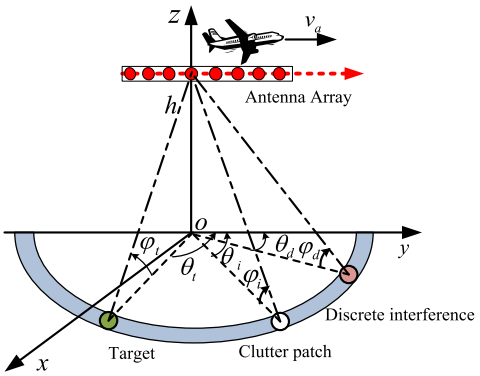


**FIGURE 1.** Configuration of a side-looking array airborne phased array radar.

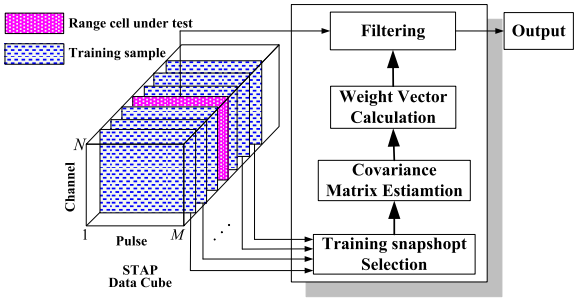


**FIGURE 2.** Procedure of STAP for airborne phased array radar.

## II. SIGNAL MODEL AND PROBLEM STATEMENT

The configuration of a side-looking airborne phased array radar is shown in Fig. 1. The $N$-element uniform linear array with inter-element spacing $d_A$ aligns with the platform motion direction. During each coherent processing interval (CPI), $M$ identical pulses are transmitted with a pulse repetition frequency (PRF) of $f_r$. The radar wavelength is $\lambda$, the height of platform is $h$ with a velocity denoted by $v_a$, and $L$ range samples are collected in each pulse repetition interval (PRI). Each CPI data of the received signal is expressed as an $N \times M \times L$ data-cube as shown in Fig. 2. Each slice of the data cube along with the range is an $N \times M$ matrix, which can be given as an $NM \times 1$ vector according to the channel order.

Assume that the $l$th range cell is under test. Then the space-time snapshot $\boldsymbol{x}_l \in \mathbb{C}^{NM\times 1}$ is given as

$$\boldsymbol{x}_l = \boldsymbol{x}_c + \boldsymbol{x}_t + \boldsymbol{x}_d + \boldsymbol{x}_n \tag{1}$$

where $\boldsymbol{x_c}$ is the clutter, $\boldsymbol{x_t}$ is the wanted target echo, $\boldsymbol{x_d}$ is the discrete interference and the noise vector $\boldsymbol{x}_n$ is assumed to be zero-mean complex Gaussian, spatially and temporally white.

According to the configuration in Fig. 1, the clutter in each range cell is the sum of $N_c$ independent clutter patches with angle interval $\Delta\varphi = 2\pi/N_c$. In each range cell, each clutter patch can be denoted by the azimuth angle $\theta$ and elevation angle $\varphi$. The normalized spatial frequency $\vartheta_{c,i}$ and the normalized Doppler frequency $\omega_{c,i}$ of the $i$th clutter patch

are respectively given as

$$\vartheta_{c,i} = \frac{d_A}{\lambda}\cos\left(\theta_{l,i}\right)\sin\left(\varphi_l\right), \quad \omega_{c,i} = \frac{2v_a}{\lambda f_r}\cos\left(\theta_{l,i}\right)\sin\left(\varphi_l\right) \tag{2}$$

Thus, the space-time steering vector of the $i$th clutter patch is given as

$$\boldsymbol{v}(\omega_{c,i}, \vartheta_{c,i}) = \boldsymbol{b}(\omega_{c,i}) \otimes \boldsymbol{a}(\vartheta_{c,i}) \tag{3}$$

where $\boldsymbol{b}(\omega_{c,i}) = [1, \exp(j2\pi\omega_{c,i}), \ldots, \exp(j(M-1)2\pi\omega_{c,i})]^T \in \mathbb{C}^{M\times 1}$ is the temporal steering vector and $\boldsymbol{a}(\vartheta_{c,i}) = [1, \exp(j2\pi\vartheta_{c,i}), \ldots, \exp(j(N-1)2\pi\vartheta_{c,i})]^T \in \mathbb{C}^{N\times 1}$ is the spatial steering vector, transposition is denoted by the superscripts $T$, and $\otimes$ represents the Kronecker product. Thus based on Melvin's model [3], the space-time clutter snapshot $\boldsymbol{x}_c \in \mathbb{C}^{NM\times 1}$ is denoted as

$$\boldsymbol{x}_c = \sum_{i=1}^{N_c} \tilde{\xi}_i \boldsymbol{v}(\omega_{c,i}, \vartheta_{c,i}) \tag{4}$$

where $\tilde{\xi}_i$ is the complex amplitude corresponding to the $i$th clutter patch. Denote the target azimuth angle is $\theta_t$ and the relative velocity as $v_t$. Then, the target echo $\boldsymbol{x}_t \in \mathbb{C}^{NM\times 1}$ is given as

$$\boldsymbol{x}_t = \tilde{\xi}_t\left(\boldsymbol{v}(\omega_t, \vartheta_t)\right) = \tilde{\xi}_t \boldsymbol{b}(\omega_t) \otimes \boldsymbol{a}(\vartheta_t) \tag{5}$$

where $\vartheta_t = d_A\cos(\theta_t)\sin(\varphi_l)/\lambda$ is the normalized spatial frequency and $\omega_t = 2v_t\cos(\theta_t)\sin(\varphi_l)/\lambda f_r$ is the normalized Doppler frequency.

Meanwhile, high towers and high-speed vehicles would often form discrete interferences in practical environment. Compared with the true target, the discrete interferences are usually located at different directions with different Doppler frequencies. Thus, the discrete interferences $\boldsymbol{x}_d \in \mathbb{C}^{NM\times 1}$ can be modeled similar with target, i.e.,

$$\boldsymbol{x}_d = \sum_{p=1}^{N_d} \tilde{\xi}_{d,p} \boldsymbol{v}(\omega_{d,p}, \vartheta_{d,p}) \tag{6}$$

where $N_d$ is the discrete interference number, $\tilde{\xi}_{d,p}$ is complex amplitude of the $p$th discrete interference and $\boldsymbol{v}(\omega_{d,p}, \vartheta_{d,p})$ is the space-time steering vector of the $p$th discrete interference. Then the weight vector $\boldsymbol{w} \in \mathbb{C}^{NM\times 1}$ of the conventional STAP is expressed as the following

$$\min_{\boldsymbol{w}} J(\boldsymbol{w}) = E\left\{\left\|\boldsymbol{w}^H\boldsymbol{x}_l\right\|_2^2\right\} \quad s.t.\ \boldsymbol{w}^H\boldsymbol{v}_t(\omega_t, \vartheta_t) = 1 \tag{7}$$

where $\boldsymbol{v}_t(\omega_t, \vartheta_t)$ is the space-time steering vector of the target, $||\boldsymbol{x}||_2$ denotes the $L_2$-norm operations of $\boldsymbol{x}$, $E\{\cdot\}$ stands for the expected value of a random variable, conjugate transposition is denoted by the superscripts $H$. Based on [1], [2], the optimal adaptive weighting vector is obtained as

$$\boldsymbol{w} = \frac{\boldsymbol{R}^{-1}\boldsymbol{v}_t(\omega_t, \vartheta_t)}{\boldsymbol{v}_t^H(\omega_t, \vartheta_t)\boldsymbol{R}^{-1}\boldsymbol{v}_t(\omega_t, \vartheta_t)} \tag{8}$$

where the space-time covariance matrix $\boldsymbol{R} \in \mathbb{C}^{NM\times NM}$ is estimated from $K$ i.i.d. training data around the $l$th range cell, i.e.,

$$\tilde{\boldsymbol{R}} = E\left\{\boldsymbol{x}\boldsymbol{x}^H\right\} \approx \frac{1}{K}\sum_{k=1,k\neq l}^{K-1} \boldsymbol{x}_k\boldsymbol{x}_k^H = \tilde{\boldsymbol{R}}_c + \tilde{\boldsymbol{R}}_n \tag{9}$$

In (9), $\tilde{\boldsymbol{R}}_c$ is the clutter covariance matrix, and $\tilde{\boldsymbol{R}}_n = \sigma^2\boldsymbol{I}$ is the noise covariance matrix with $\sigma^2$ denotes the noise power and $\boldsymbol{I}$ is the $NM\times NM$ identity matrix. Afterwards, the test statistic can be obtained for target detection.

$$\boldsymbol{y}_l = \frac{\left|\boldsymbol{w}^H\boldsymbol{x}_l\right|^2}{\boldsymbol{w}^H\boldsymbol{R}\boldsymbol{w}} = \frac{\left|\boldsymbol{v}_t^H(\omega_t, \vartheta_t)\boldsymbol{R}^{-1}\boldsymbol{x}_l\right|^2}{\boldsymbol{v}_t^H(\omega_t, \vartheta_t)\boldsymbol{R}^{-1}\boldsymbol{v}_t(\omega_t, \vartheta_t)} \tag{10}$$

It is obvious that the discrete interference is absent in the training data thus it cannot be suppressed adaptively. The hybrid method of STAP method and the DDD method were proposed to suppress both the homogeneous clutter and the discrete interference [6]–[8]. However, this method still requires a large number of i.i.d. training data for the clutter covariance matrix estimation, which is hard to realize in a practical clutter environment. This fact motivates us to develop a new method that robustly suppresses both clutter and discrete interference in a real clutter environment.

## III. CLUTTER SPARSITY AND SPARSITY-BASED RECOVERY

### A. CLUTTER SPARSITY ANALYSIS

It is well known that the space-time covariance matrix $\boldsymbol{R}$ can be expressed in the following way [30]

$$\boldsymbol{R} = \boldsymbol{U}_c\boldsymbol{\Lambda}_c\boldsymbol{U}_c^H + \sigma^2\boldsymbol{U}_n\boldsymbol{U}_n^H \tag{11}$$

where $\boldsymbol{U}_c$ is the clutter subspace consisting of the principal eigenvectors, $\Lambda_c = \mathrm{diag}(\varsigma_1, \ldots, \varsigma_P)$ is the diagonal matrix consisting of the $P$ principal eigenvalues of $\boldsymbol{R}$, and $\boldsymbol{U}_n$ is the noise subspace. Therefore, the clutter covariance matrix can be denoted by only the $P$ principal eigenvalues instead of the $N_c$ space-time steering vectors according to the clutter model in Section II, thus the clutter is sparse in terms of the spatial-temporal system degrees of freedom (DoFs). In order to demonstrate the sparsity of clutter, the space-time correlation coefficient is given as

$$cor\left(\mathbf{v}(\omega_i, \vartheta_i), \mathbf{v}(\omega_j, \vartheta_j)\right) = \frac{\left\|\mathbf{v}(\omega_i, \vartheta_i)^H\mathbf{v}(\omega_j, \vartheta_j)\right\|}{\left\|\mathbf{v}(\omega_i, \vartheta_i)\right\| \cdot \left\|\mathbf{v}(\omega_j, \vartheta_j)\right\|} \tag{12}$$

It describes the degree of correlation between different space-time steering vectors. The correlation coefficients corresponding to three different spatial angles are shown in Fig. 3. It is seen that the space-time steering vector is highly correlated to the vectors which are spatially adjacent. It means that the clutter has a high correlation with components separated by a close spatial angle, and the space-time steering vector closed to the clutter ridge can replace all the vectors in the spatial-temporal plane to approximate the clutter [28]. Therefore the space-time data shows high sparse distribution

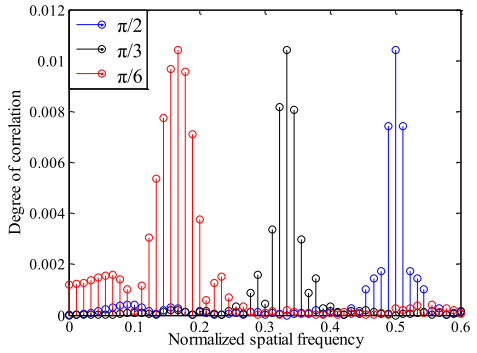


**FIGURE 3.** Correlations between space-time steering vectors with spatial angle $\pi/2$, $\pi/3$, and $\pi/6$.

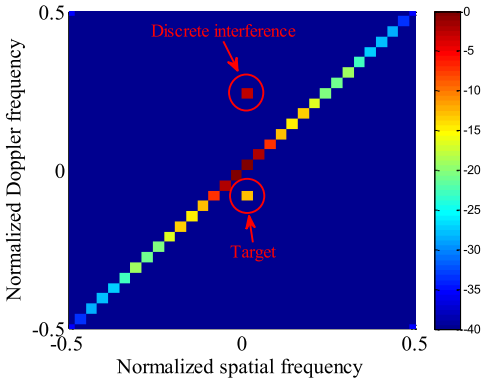


**FIGURE 4.** Sparse distribution of spatial-temporal spectrum in angle-Doppler domain.

property in the angle-Doppler domain [13]–[15]. As shown in Fig. 4, the prominent components of clutter spectrum are distributed near the clutter ridge, and the discrete interferers and possible target are located dispersedly. It is evident that the amplitude of the spectrum in most area is rather small, showing sparse in the angle-Doppler domain.

### B. SPARSITY-BASED CLUTTER SPECTRUM RECOVERY

Based on the sparse property, the homogeneous clutter and discrete interference can be effectively estimated by the sparse recovery methods. The spatial-temporal plane is discretized into a grid consists of $N_s$ spatial bins and $N_d$ Doppler bins, where each grid point is associated with the specific space-time steering vector $\boldsymbol{v}\left(\omega_{d,i}, \vartheta_{s,j}\right)$ $(i = 1, .., N_d, j = 1, .., N_s)$ [13]. Therefore the space-time snapshot can be rewritten as

$$\boldsymbol{x}_l = \boldsymbol{x}_c + \boldsymbol{x}_t + \boldsymbol{x}_d + \boldsymbol{x}_n = \Phi\gamma + \boldsymbol{x}_n \tag{13}$$

where $\boldsymbol{\gamma} = \left[\tilde{\gamma}_{1,1}, \tilde{\gamma}_{1,2}, \ldots, \tilde{\gamma}_{N_s,N_d}\right]^T \in \mathbb{C}^{N_sN_d\times 1}$ is the complex amplitude of the spectral distribution. The overcomplete space-time dictionary matrix $\Phi \in \mathbb{C}^{NM\times N_sN_d}$ denotes the collection of all space-time steering vectors, i.e.,

$$\Phi = \left[\boldsymbol{v}\left(\omega_{d,1}, \vartheta_{s,1}\right), \ldots, \boldsymbol{v}\left(\omega_{d,i}, \vartheta_{s,j}\right), \ldots, \boldsymbol{v}\left(\omega_{d,N_d}, \vartheta_{s,N_s}\right)\right] \tag{14}$$

Therefore, by estimating the complex amplitude of the spectral distribution and the corresponding space-time steering vectors their sparsity based on their sparsity, $\boldsymbol{R}$ can be reconstructed for the clutter suppression. As $N_sN_d$ is much larger than $NM$, the space-time dictionary $\Phi$ is overcomplete, thus (13) is underdetermined. However, based on the theory of sparse recovery processing [31], [32], this ill-posed problem can be solved effectively by the technique of sparse representation with few training data

$$\begin{aligned}\hat{\boldsymbol{\gamma}} = &\arg\min \|\boldsymbol{\gamma}\|_1 \\ &\text{subject to } \|\mathbf{x}_l - \boldsymbol{\Phi\gamma}\|_2 \le \varepsilon\end{aligned} \tag{15}$$

where $||\boldsymbol{x}||_1$ denotes the $L_1$-norm operations of $\boldsymbol{x}$. The $L_1$-norm guarantees the sparsity of $\gamma_l$, and the $L_2$-norm restrains the estimation error within $\varepsilon$. (15) can also be reformulated as

$$\hat{\boldsymbol{\gamma}} = \arg\min_{\boldsymbol{\gamma}} \|\mathbf{x}_l - \boldsymbol{\Phi\gamma}\|_2 + \lambda_\gamma \|\boldsymbol{\gamma}\|_1 \tag{16}$$

where $\lambda_\gamma$ is the regularization parameter. The spatial-temporal clutter spectrum can be obtained by averaging each results of $\boldsymbol{\gamma}$, and then $\boldsymbol{R}$ can be constructed for calculating the adaptive weighting vectors correspondingly.

The computational complexity of conventional sparsity-based STAP methods based on the $L_1$-norm optimization is on the order of $O((N_sN_d)^3)$, which is impractical for practical application [8]. Several fast approximation methods can be used to reduce the complexity. In the FOCUSS method [14], [16], based on the weighted $L_2$-norm optimization, the spectrum is iteratively estimated by using Lagrange multipliers. However, the regularization parameter in the FOCUSS method cannot be adjusted dynamically according to the received data, thereby degrading the estimation under practical environments.

In recent years, the sparse recovery problem is developed by the SBL processing based on the MAP and RVM principle [23]. The MAP method optimizes the multi-variable objective function iteratively by maximizing the joint PDF. On other hand, the RVM method can obtain desirable performance, but the computational complexity of determining hyper-parameter is extremely high, making it very difficult for practical application. Motivated by this, in the next subsection, we propose a robust STAP method based on the MAP principle by investigating the sparsity of the clutter and discrete interference [25]–[27].

## IV. PROPOSED DISCRETE INTERFERENCE SUPPRESSION METHOD BASED ON ROBUST BAYESIAN COMPRESSIVE SENSING

In order to avoid the target being suppressed as a discrete interference, the target echo should be firstly removed by the orthogonal projection before performing the discrete interference suppression [33], i.e.,

$$\tilde{\boldsymbol{x}}_l = \boldsymbol{B}\boldsymbol{x}_l \tag{17}$$

where $\boldsymbol{B} = \boldsymbol{I} - \boldsymbol{V}\left(\boldsymbol{V}^H\boldsymbol{V}\right)^{-1}\boldsymbol{V}$ denotes the orthogonal blocking matrix, $\boldsymbol{V} = \left[\boldsymbol{v}\left(\omega_{d,i-\tilde{N}}, \vartheta_{s,j-\tilde{N}}\right), \ldots, \boldsymbol{v}\left(\omega_{d,i}, \vartheta_{s,j}\right), \ldots, \boldsymbol{v}\left(\omega_{d,i+\tilde{N}}, \vartheta_{s,j+\tilde{N}}\right)\right]$, $\boldsymbol{v}\left(\omega_{d,i}, \vartheta_{s,j}\right) = \boldsymbol{v}_t^H(\omega_t, \vartheta_t)$ denotes the set of spatial-temporal steering vectors covering the region of interest, and $\tilde{N}$ decides the number of the spatial-temporal steering vectors for constructing the block matrix. Because clutter may not be exactly located exactly on a gird point of the dictionary, thus in order to further improve the estimation performance, the off-grid mismatch between the space-time overcomplete dictionary and the actual clutter distribution needs to be considered [17], [34], [35]. In the proposed method, the space-time snapshot of the range cell under test is rewritten as

$$\tilde{\boldsymbol{x}}_l = \boldsymbol{x}_c + \boldsymbol{x}_d + \boldsymbol{x}_n = \Theta\boldsymbol{\gamma} + \boldsymbol{x}_n \tag{18}$$

where the actual overcomplete dictionary is $\boldsymbol{\Theta} = \boldsymbol{\Phi} + \boldsymbol{\Lambda}\boldsymbol{\Phi}$ and the mismatch matrix is $\boldsymbol{\Lambda}$. Then the sparse recovery of clutter and discrete interference becomes

$$\hat{\boldsymbol{\gamma}} = \arg\min_{\boldsymbol{\gamma}} \|\tilde{\boldsymbol{x}}_l - \boldsymbol{\Theta}\boldsymbol{\gamma}\|_2 + \lambda_\gamma \|\boldsymbol{\gamma}\|_1 \tag{19}$$

Based on the above formulations, the estimation of the clutter spectrum and the calibration of overcomplete dictionary error are achieved iteratively. The details of the proposed method are provided in the following two subsections.

### A. SPARSE RECOVERY OF SPATIAL-TEMPORAL SPECTRUM

As known in [26] and [27], the likelihood of a space-time snapshot in (18) can be given as

$$\begin{aligned} &\tilde{\boldsymbol{x}}_l \sim \boldsymbol{CN}\left(\Theta\boldsymbol{\gamma}, \eta\boldsymbol{I}\right) \\ &p\left(\tilde{\boldsymbol{x}}_l|\boldsymbol{\gamma}, \eta\right) = (2\pi\eta)^{NM}\exp\left(-\frac{\|\tilde{\boldsymbol{x}}_l - \Theta\boldsymbol{\gamma}\|_2^2}{2\eta}\right) \\ &p(\eta) \propto 1 \end{aligned} \tag{20}$$

where $p\left(\tilde{\boldsymbol{x}}_l|\boldsymbol{\gamma}, \eta\right)$ is a sparsity promoting prior, and $\eta$ denotes the estimated noise power with the probability over the range $[0, \infty)$ [27], [28]. The complex amplitude $\gamma$ is subject to the Laplace prior distribution

$$p\left(\boldsymbol{\gamma}|\kappa\right) = \frac{\kappa}{2}\exp\left(-\frac{\kappa}{2}\|\boldsymbol{\gamma}\|_1\right) \tag{21}$$

where $\kappa$ is the parameter that represents the sparsity of $\boldsymbol{\gamma}$. Based on the MAP principle, the spares recovery solution in (19) can be given as

$$\boldsymbol{\gamma}_{MAP} = \arg\max_{\boldsymbol{\gamma}}\left(p\left(\tilde{\boldsymbol{x}}_l, \boldsymbol{\gamma}, \eta|\kappa\right)\right) \tag{22}$$

Because $p\left(\tilde{\boldsymbol{x}}_l, \boldsymbol{\gamma}, \eta|\kappa\right) \propto p\left(\tilde{\boldsymbol{x}}_l, \boldsymbol{\gamma}, \eta, \kappa\right)$, (22) is equivalent to

$$\begin{aligned} \boldsymbol{\gamma}_{MAP} &= \arg\max_{\boldsymbol{\gamma}}\left(p\left(\tilde{\boldsymbol{x}}_l, \boldsymbol{\gamma}, \eta|\kappa\right)\right) \\ &= \arg\max_{\boldsymbol{\gamma}}\left(p\left(\tilde{\boldsymbol{x}}_l|\boldsymbol{\gamma}, \eta\right)p\left(\tilde{\boldsymbol{x}}_l|\kappa\right)p(\eta)\right) \\ &= \arg\max_{\boldsymbol{\gamma}}\left((2\pi\eta)^{-NM}\exp\left(-\frac{\|\tilde{\boldsymbol{x}}_l - \boldsymbol{\Theta}\boldsymbol{\gamma}\|_2^2}{2\eta}\right)\right. \\ &\quad \left.\times\frac{\kappa}{2}\exp\left(-\frac{\lambda}{2}\|\boldsymbol{\gamma}\|_1\right)\right) \end{aligned} \tag{23}$$

Maximizing the log-likelihood function yields

$$\begin{aligned} \arg\min_{\boldsymbol{\gamma}} J\left(\boldsymbol{\gamma}, \eta\right) &= \arg\max_{\boldsymbol{\gamma}}\left(-\ln\left(\tilde{\boldsymbol{x}}_l, \boldsymbol{\gamma}, \eta|\kappa\right)\right) \\ &= \arg\max_{\boldsymbol{\gamma}}\left(NM\ln(2\pi\eta) + \frac{\|\tilde{\boldsymbol{x}}_l - \boldsymbol{\Theta}\boldsymbol{\gamma}\|_2^2}{2\eta}\right. \\ &\quad \left.-\ln\frac{\kappa}{2} + \frac{\lambda}{2}\|\boldsymbol{\gamma}\|_1\right) \end{aligned} \tag{24}$$

According to [27], the objective function can be given as

$$J\left(\boldsymbol{\gamma}, \eta\right) = NM\ln(2\pi\eta) + \frac{\|\tilde{\boldsymbol{x}}_l - \boldsymbol{\Theta}\boldsymbol{\gamma}\|_2^2}{2\eta} - \ln\frac{\kappa}{2} + \frac{\lambda}{2}\|\boldsymbol{\gamma}\|_1 \tag{25}$$

Therefore when $\boldsymbol{\gamma}$ is subject to the Laplace prior distribution, the SBL based on the MAP is equivalent to $L_1$-norm optimization. Afterwards, the sparse recovery result of the spatial-temporal spectrum is achieved iteratively. In practice, the initial value of $\boldsymbol{\gamma}$ is assumed as the result of the Fourier spectrum estimation, i.e. $\boldsymbol{\gamma}_{(0)} = \boldsymbol{\Phi}^H\tilde{\boldsymbol{x}}_l$, and then at the estimations at the $k$th iteration, $\boldsymbol{\gamma}_{(k)}$ and $\eta_{(k)}$ will be computed iteratively. By fixing $\eta_{(k-1)}$, the complex amplitude $\boldsymbol{\gamma}$ at the $k$th iteration is obtained by solving the gradient equation as follow [26]

$$\begin{aligned} &\left(d\Big/d\boldsymbol{\gamma}^H\right)J\left(\boldsymbol{\gamma}, \eta_{(k-1)}\right) \\ &= \frac{\boldsymbol{\Theta}_{(k-1)}^H\boldsymbol{\Theta}_{(k-1)}\boldsymbol{\gamma}}{2\eta_{(k-1)}} - \frac{\boldsymbol{\Theta}_{(k-1)}^H\tilde{\boldsymbol{x}}_l}{2\eta_{(k-1)}} + \boldsymbol{W}_{(k-1)}\boldsymbol{\gamma} = 0 \end{aligned} \tag{26}$$

where $\boldsymbol{W}_{(k-1)} = \mathrm{diag}\left(|\gamma_1|_{(k-1)}, \ldots, |\gamma_{N_sN_d}|_{(k-1)}\right)$. Thus $\boldsymbol{\gamma}$ is updated as

$$\boldsymbol{\gamma}_{(k)} = \boldsymbol{W}_{(k-1)}\boldsymbol{\Theta}_{(k)}^H\left(\boldsymbol{\Theta}_{(k)}\boldsymbol{W}_{(k-1)}\boldsymbol{\Theta}_{(k)}^H + \eta_{(k-1)}\boldsymbol{I}\right)^{-1}\tilde{\boldsymbol{x}}_l \tag{27}$$

Then the noise $\eta$ can be updated by the same processing

$$\left(d\Big/d\eta\right)\left(J\left(\boldsymbol{\gamma}_{(k)}, \eta\right)\right) = \frac{NM}{\eta} - \frac{\left\|\tilde{\boldsymbol{x}} - \boldsymbol{\Theta}_{(k)}\boldsymbol{\gamma}_{(k)}\right\|_2^2}{\eta^2} = 0 \tag{28}$$

Thus the noise $\eta$ can be calculated as

$$\eta_{(k)} = \frac{\left\|\tilde{\boldsymbol{x}} - \boldsymbol{\Theta}_{(k)}\boldsymbol{\gamma}_{(k)}\right\|_2^2}{NM} \tag{29}$$

The estimation of the clutter spectrum can be executed iteratively according to (27) and (29). In the SBL, the PDF of the spatial-temporal spectrum is given to reduce the uncertainty error during the estimation, and the number of local minimum is much smaller than FOCUSS method [26]. Moreover, the noise vector $\eta$ can be adjusted adaptively, thus the

proposed method can provide improved performance compared with the FOCUSS method. Comparing with the sparse learning processing based on the RVM, the proposed method does not require the computation of the hyper-parameters, and therefore less computational complexity is demanded.

### B. MISMATCH CALIBRATION OF SPATIAL-TEMPORAL SPECTRUM

After getting $\boldsymbol{\gamma}_{(k)}$ at the $k$th iteration, the overcomplete space-time dictionary is calibrated at the beginning of the $k$th iteration as

$$\boldsymbol{\Theta}_{(k)} = \boldsymbol{\Phi} + \boldsymbol{\Lambda}_{(k-1)}\boldsymbol{\Phi} \tag{30}$$

Then the mismatch matrix $\boldsymbol{\Lambda}$ can be obtained according to the objective function [29], which is expressed as

$$\boldsymbol{\Lambda} = \arg\min_{\boldsymbol{\Lambda}} J(\boldsymbol{\Lambda}) = \|\boldsymbol{\Lambda}\boldsymbol{\Phi}\|_2 + \left\|\tilde{\boldsymbol{x}}_l - \boldsymbol{\Theta}_{(k)}\boldsymbol{\gamma}_{(k)}\right\|_2 \tag{31}$$

By defining $\boldsymbol{e}_{(k)} = \tilde{\boldsymbol{x}}_l - \boldsymbol{\Phi}\boldsymbol{\gamma}_{(k)}$, and $\boldsymbol{p}_{(k)} = \boldsymbol{\Phi}\boldsymbol{\gamma}_{(k)}$, the objective function of (30) can be given as

$$J(\boldsymbol{\Lambda}) = \|\boldsymbol{\Lambda}\boldsymbol{\Phi}\|_2 + \left\|\boldsymbol{e}_{(k)} - \boldsymbol{\Lambda}\boldsymbol{p}_{(k)}\right\|_2 \tag{32}$$

Minimizing the above cost function yields $\boldsymbol{\Lambda}$

$$\boldsymbol{\Lambda}_{(k)} = \boldsymbol{e}_{(k)}\left(\boldsymbol{p}_{(k)}\right)^H\left(\boldsymbol{p}_{(k)}\left(\boldsymbol{p}_{(k)}\right)^H + \boldsymbol{\Theta}_{(k)}\boldsymbol{\Theta}_{(k)}^H\right)^{-1} \tag{33}$$

As such, the overcomplete dictionary can be calibrated iteratively by minimizing the cost function, thus the error between the dictionary and the real clutter distribution is reduced effectively. Compared with the mismatch calibration method in [35], the constraint conditions of mismatch calibration in the proposed method is less, the proposed method does not need to set the range of mismatch parameters, thus it is much more convenient to be applied.

It should be noticed from (27) and (33) that the matrix inversion is still needed in each iteration, which will significantly compromise the convergence performance. However, during the iterations, the prominent components in $\boldsymbol{\gamma}$ are gradually reinforced, while the remaining small components gradually approach to zero, resulting in asymptotically negligible influence on the recovery performance. Therefore, it is unnecessary to calculate the small components in each iteration processing. In order to reduce the computational complexity, the complex amplitude $\boldsymbol{\gamma}$ can be updated based on a specific threshold, which is expressed as

$$\boldsymbol{\Gamma} = \left\{\gamma_i \in \boldsymbol{\gamma}_{(k)} : |\gamma_i| \geq Th\right\}, \quad i = 1, 2, \ldots, N_s N_d \tag{34}$$

where $\boldsymbol{\gamma}_{(k)}$ is obtained at the $k$th iteration, $Th$ is the specific updating threshold for selecting the complex amplitude and the column in the dictionary $\boldsymbol{\Theta}$ to be updated in the subsequent iteration, and $\boldsymbol{\Gamma}$ records the indices of elements over the threshold. Based on the specific threshold, the matrix inversion does not need to incorporate the entire dictionary, thereby significantly reducing the computational complexity

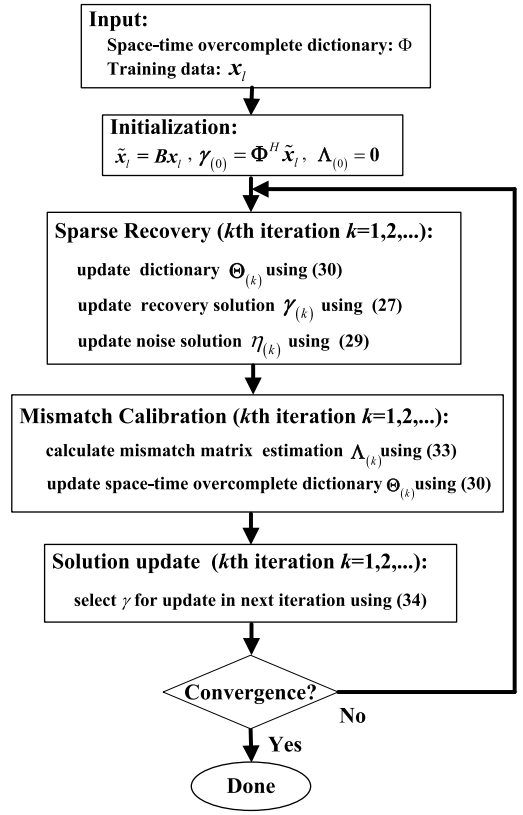


**FIGURE 5.** Processing procedure of the proposed robust SBL method (R-SBL).

compared with the method given in [17]. Afterwards, the iteration continues until the convergence condition $\xi$ is satisfied.

$$\left|\frac{\boldsymbol{\gamma}_{(k)} - \boldsymbol{\gamma}_{(k-1)}}{\boldsymbol{\gamma}_{(k)}}\right| \leq \xi \tag{35}$$

The processing procedure of the proposed method, referred to as the robust SBL method (R-SBL), is summarized in Fig. 5. In order to obtain a better estimation of the clutter and the discrete interference profiles, several snapshots of adjacent range cell can be utilized in the same processing. Afterwards, the covariance matrix $\boldsymbol{R}$ can be reconstructed as

$$\boldsymbol{R} = \frac{1}{P}\sum_{p=1}^{P}\sum_{i=1}^{N_d}\sum_{j=1}^{N_s}\left|\tilde{\gamma}_{p,i,j}\right|^2 \boldsymbol{v}_p\left(\omega_{d,i}, \vartheta_{s,j}\right)\boldsymbol{v}_p^H\left(\omega_{d,i}, \vartheta_{s,j}\right) + \sigma^2\boldsymbol{I} \tag{36}$$

where $P$ is the number of training snapshot, $\boldsymbol{v}_p\left(\omega_{d,i}, \vartheta_{s,j}\right)$ is the space-time steering vector in the overcomplete dictionary corresponding to the recovery result of each training data. Then the weight vector $\boldsymbol{w}$ and detection test statistic can be obtained according to (9) and (10) accordingly. Because of the robust estimation of the clutter and discrete interference profiles, the discrete interference and the clutter component can be both effectively estimated.

**TABLE 1. The computational complexity of M-FOCUSS, SBL, G-SBL, FB-SBL and proposed R-SBL methods.**

| Method | Computational complexity |
|---|---|
| M-FOCUSS | $O\left(\sum_{i=1}^{K_{FOCUSS}}\left(D_{FOCUSS,i}\right)^3\right)$ |
| SBL | $O\left(\sum_{i=1}^{K_{SBL}}\left(D_{SBLi}\right)^3\right)$ |
| G-SBL | $O\left(\sum_{i=1}^{K_{G-SBL}}\left(D_{G-SBL,i}\right)^3\right)$ |
| FB-SBL | $O\left(\sum_{i=1}^{K_{FB-SBL}}\left(D_{FB-SBL,i}\right)^3\right)$ |
| R-SBL | $O\left(\sum_{i=1}^{K_{R-SBL}}\left(D_{R-SBL,i}\right)^3\right)$ |

**TABLE 2. Simulation parameters.**

| Parameter | Value |
|---|---|
| Elements number | 8 |
| Pulses number | 12 |
| Radar frequency | 1.2GHz |
| Platform velocity | 100m/s |
| Pulse repetition frequency | 1600Hz |
| Platform height | 12km |
| Number of range cell | 160 |
| Channel spacing | $\lambda/2$ |
| Target normalized Doppler frequency | -0.15 |
| Target power | 0dB |
| Discrete interference normalized Doppler frequency | 0.24 |
| Discrete interference-to-noise ratio | 40dB |
| Clutter-to-noise ratio | 40dB |
| Number of tested range cells | 80 |

## V. COMPUTATIONAL COMPLEXITY ANALYSIS

In this section, the computational complexity of the proposed R-SBL method is investigated and compared with some sparsity-based STAP methods such as the M-FOCUSS method [16], the G-SBL method [21], the FB-SBL method [37] and the SBL method without error calibration [26]. The computational complexity of the M-FOCUSS, SBL, G-SBL, FB-SBL and R-SBL methods are summarized in Table 1, where $N_s$ and $N_d$ are the numbers of spatial and Doppler bins, $K_{FOCUSS}$, $K_{SBL}$, $K_{G\text{-}SBL}$, $K_{FB\text{-}SBL}$ and $K_{R\text{-}SBL}$ are respectively the numbers of iterations of the M-FOCUSS, SBL, G-SBL, FB-SBL and proposed R-SBL method, and $D_{FOCUSS}$, $D_{SBL}$, $D_{G\text{-}SBL}$, $D_{FB\text{-}SBL}$ and $D_{R\text{-}SBL}$ are the numbers of updated elements at each iteration for the‘ four methods. Note that, as the $L_1$-norm optimization by the convex optimization [16], [17] has already been discussed in a number of papers and its computational complexity is much larger than that of other sparsity-based STAP methods, thus it is not included in the comparison. In the simulations, $N_s = 6N$ and $N_d = 6M$, the number of DoFs $NM$ ranges from 16 to 256, All the results are averaged over 500 Monte Carlo simulations. The other simulation parameters are listed in Table 2 in the next section.

It can be found from Table 1 that the total computational complexity of all the methods are determined by the iteration numbers required in each iteration. As shown in Fig. 6, because of the robust sparse recovery processing, the proposed method can achieve convergence with the least number of iterations. On other hand, due to a lack of the mismatch calibration, the SBL method requires more iterations compared with the proposed method and the M-FOCUSS method. It should be aware that the G-SBL method and FB-SBL method need to add (or delete) atoms to the model until all relevant atoms are included for reconstruction, thus more iterations are needed, and the FB-SBL method uses

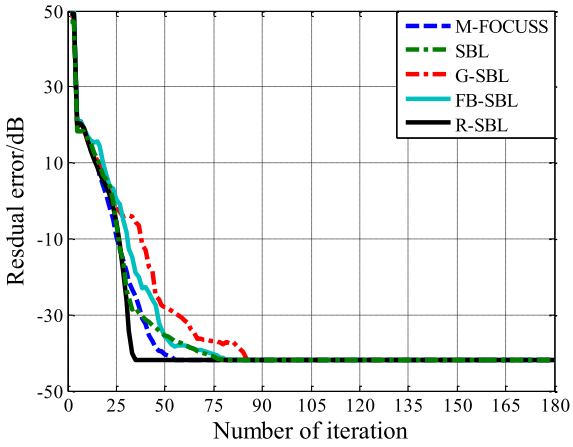


**FIGURE 6. The residual error of M-FOCUSS, SBL, G-SBL, FB-SBL and proposed R-SBL methods versus the number of iterations.**

the block sparsity and the intra-correlation of the sparse signal [37], [38], the number of iterations can be reduced.

The computational complexity is simulated and the corresponding results are shown in Fig. 7. It can be found that the G-SBL method costs the most computational complexity, the FB-SBL method uses the block sparsity and the intra-correlation of the sparse signal, thus the computational complexity is reduced compared with the G-SBL method. On the contrast, the computational complexity of the proposed method is lower than G-SBL and FB-SBL methods because of the least number of iterations. According to the simulation, when the number of DoFs is 128, the computational complexity of G-SBL method and FB-SBL method is $1.463 \times 10^4$ MFLOPs and $1.162 \times 10^4$ MFLOPs respectively and the computational complexity of the proposed method is $0.942 \times 10^4$ MFLOPs. That is, the computational complexity of the proposed method is reduced by about 55%

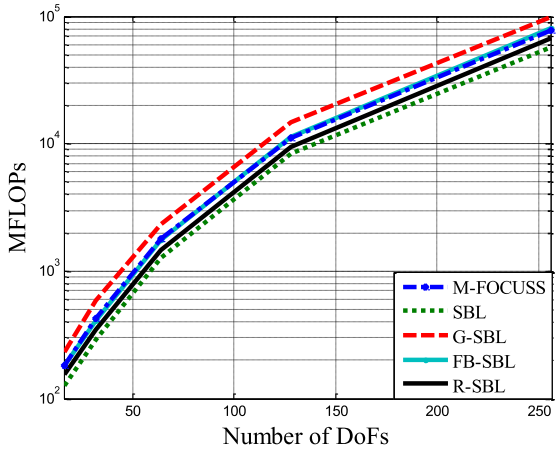


**FIGURE 7.** Computational complexity of M-FOCUSS, SBL, G-SBL, FB-SBL and proposed R-SBL methods.

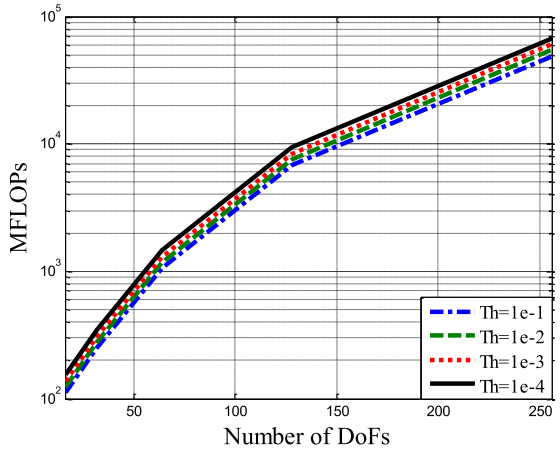


**FIGURE 8.** Computational complexity of the proposed R-SBL method versus different updating thresholds *Th*.

and 23%. Meanwhile, the proposed method and the M-FOCUSS method require nearly the same computational complexity. As shown in the next section, however, the proposed method provides better performance.

Moreover, as the proposed method utilizes the threshold to accelerate the iteration processing, thus the computational complexity versus the different updating thresholds *Th* is also analyzed and the corresponding results are shown in Fig. 8. It can be found that when the threshold *Th* is small, the dimension of sparse recovery is huge, thus it costs more computations. On the other hand, when the threshold *Th* is too large, a large number of elements would be disregarded, thus the computational complexity is reduced. However, it should be noticed that much elements would be undesirably disregarded by inappropriate threshold, which would lead to degraded reconstruction performance, therefore the threshold should be carefully set in practical application, the clutter performance against different thresholds will be analyzed in the next section.

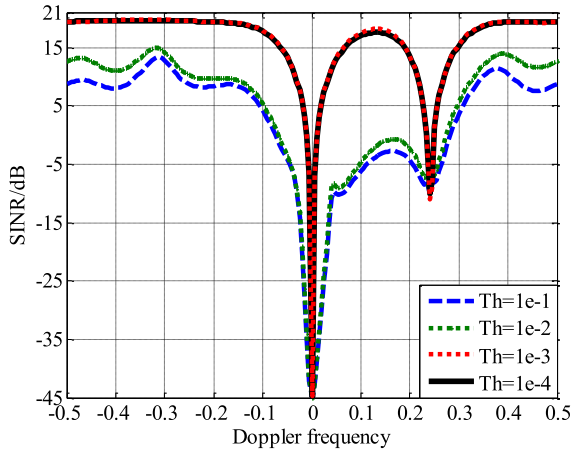


**FIGURE 9.** Output SINRs of proposed method versus different updating thresholds *Th*.

## VI. CLUTTER SUPPRESSION PERFORMANCE

In this section, by using the simulated data, the MCARM data, and one actual measured airborne phased array radar data, the performance of the proposed method is investigated and compared with the M-FOCUSS method, conventional SBL method and the G-SBL method. The output SINR is employed as the metric for the performance comparisons, when the target power is denoted as $\sigma_t^2 = E\left\{\left|\tilde{\xi}_t\right|^2\right\}$, the output SINR is defined as

$$SINR_{out} = \frac{\sigma_t^2 |\boldsymbol{w}^H \boldsymbol{v}_t(\omega_t, \vartheta_t)|^2}{\boldsymbol{w}^H \boldsymbol{R} \boldsymbol{w}} \tag{37}$$

### A. SIMULATED DATA

The performance verification is firstly carried out by a simulated side-looking ULA array. The simulation data is generated based on Melvin's model [3] and the detailed parameters are listed in Table 2. In the simulations, the noise power is assumed to be 0dBm, the number of spatial bins is $N_s = 6N$ and the number of Doppler bins is $N_d = 6M$, and all results are averaged over 500 Monte Carlo runs.

#### 1) EFFECT OF UPDATING THRESHOLD

Firstly, as the updating threshold is used in the proposed method, the SINR output of the proposed method versus the updating thresholds in each iteration should be simulated accordingly and the corresponding results are shown in Fig. 8. It is found that the SINR degrades when the threshold *Th* is selected inappropriately. When the threshold *Th* is too small, the dimension of sparse recovery is huge, thus it costs more computations. On the other hand, when the threshold *Th* is too large, a large number of elements would be undesirably disregarded, leading to degraded reconstruction performance. It can be found from Fig. 9 that the proposed method provides desirable performance when the threshold *Th* is about 1e-3 time of the noise level, which is applied in the following simulations.

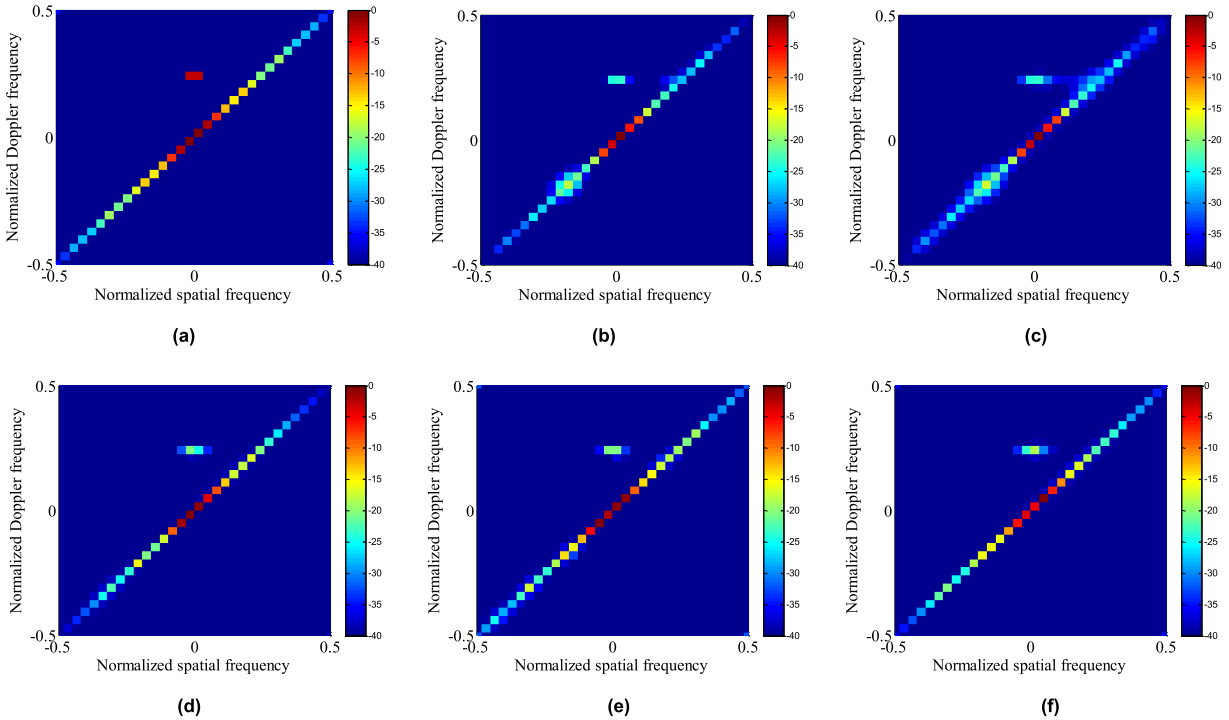


**FIGURE 10.** Sparse recovery performance of spatial-temporal spectrum. (a) Optimum results. (b) M-FOCUSS method. (c) SBL method. (d) G-SBL method. (e) FB-SBL method. (f) Proposed R-SBL method.

### 2) SPARSE RECOVERY PERFORMANCE OF SPATIAL-TEMPORAL SPECTRUM

The sparse recovery performance of the spatial-temporal spectrum obtained by the proposed method is simulated and compared with the M-FOCUSS method, SBL method, G-SBL method, FB-SBL method and the optimum spatial-temporal spectrum. The corresponding results are shown in Fig. 10. It is observed that the target profile is removed by all the methods because of the orthogonal projection processing. The spatial-temporal spectrum obtained by the M-FOCUSS and conventional SBL methods are spread and contain some false peaks, which will affect the clutter suppression performance. On the other hand, the proposed method, the G-SBL method and the FB-SBL method obtain similar spectrum to the optimum result. However, the G-SBL method costs more computational complexity than the proposed method.

### 3) PERFORMANCE OF CLUTTER AND DISCRETE INTERFERENCE SUPPRESSION

The output SINR of the proposed method is simulated with respect to the number of training data and compared with the M-FOCUSS method, G-SBL method, and SBL method. The results are shown in Fig. 11. It is clear that the proposed method outperforms the M-FOCUSS and the conventional SBL methods. Meanwhile, comparing with the G-SBL method and the FB-SBL method, the proposed R-SBL method can achieve comparable performance with less computational complexity cost, which is shown and analyzed in the previous section.

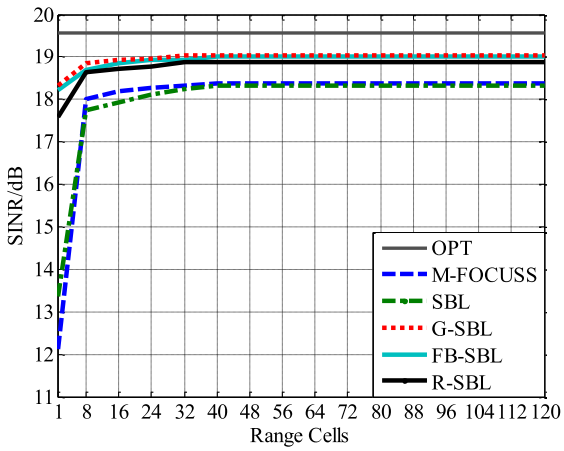


**FIGURE 11.** Output SINRs of M-FOCUSS, SBL, G-SBL and proposed R-SBL methods versus the number of training data.

Then the output SINRs by 4 training data and the range detection performance at target normalized Doppler frequency are simulated and the corresponding results are shown in Fig. 12 and Fig 13. It is found that all sparsity-based methods can effectively suppress the clutter and discrete interference, thus the proposed method can obtain better suppression performance than M-FOCUSS method and SBL method because of the robust iterative sparse recovery processing. Meanwhile, comparing with the G-SBL method

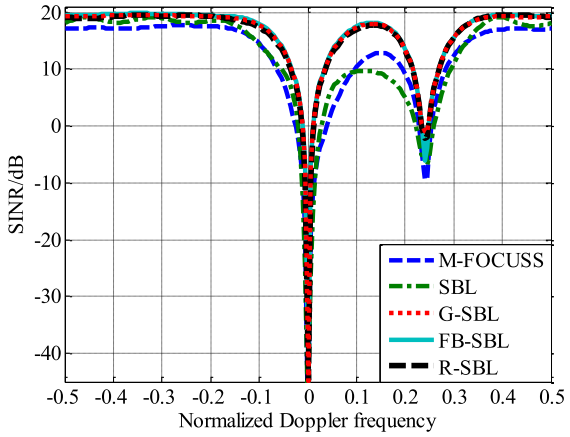


**FIGURE 12.** Output SINRs of M-FOCUSS, SBL, G-SBL, FB-SBL and proposed R-SBL methods versus the target Doppler frequency.

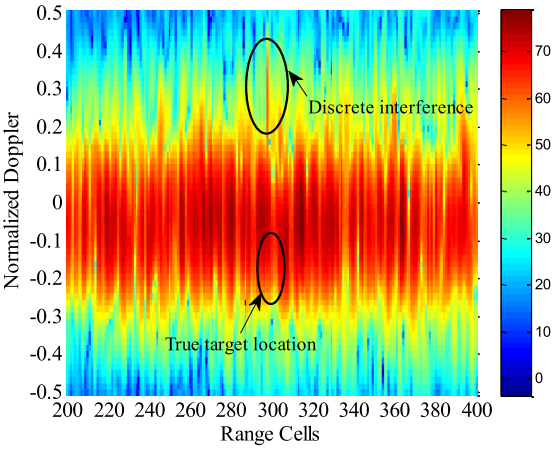


**FIGURE 14.** The range-Doppler spectrum of MCARM data.

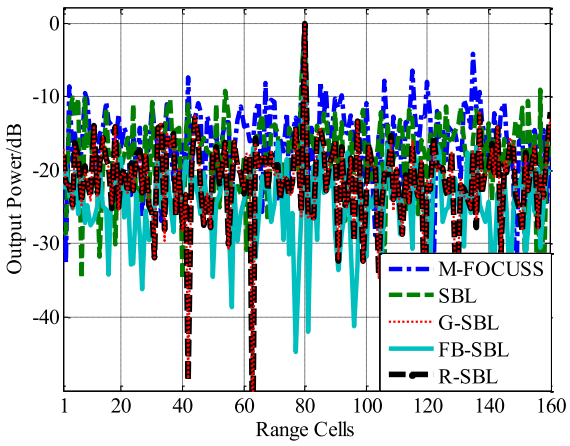


**FIGURE 13.** Range detection performance at target Doppler frequency of M-FOCUSS, SBL, G-SBL, FB-SBL and proposed R-SBL methods.

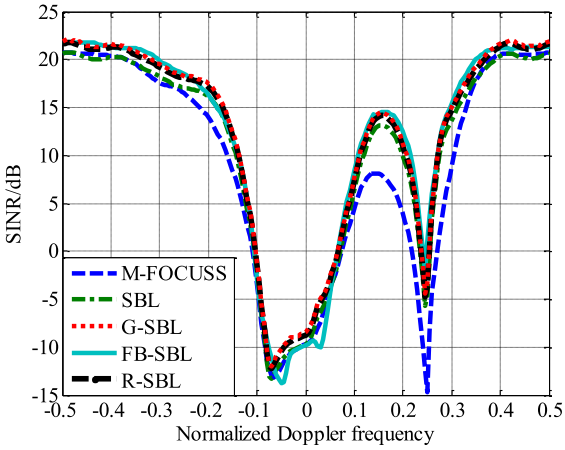


**FIGURE 15.** Output SINRs of M-FOCUSS, SBL, G-SBL, FB-SBL and proposed R-SBL methods based on MCARM data.

and FB-SBL method, comparable performance is obtained by the proposed method, a desirable range detection performance is achieved.

### *B. MEASURED DATA*

In this section, by utilizing the MCARM data and the actual measured airborne radar data, the proposed R-SBL method is verified and compare with the M-FOCUSS, G-SBL, FB-SBL and conventional SBL methods.

#### 1) MCARM DATA

In this example, the MCARM data is utilized for verification [36]. The array was an L-band phased array antenna consisting of 22 elements arranged as $2\times11$ configuration. The PRF of the radar is 1984Hz, the platform velocity is 100m/s, and the platform height is 3078m. 12 pulses and 8 elements data are applied. It is known from [36] that a target is located at the 299th range cell with a normalized Doppler frequency of -0.15. A made discrete interference is inserted in the CUT, whose INR is set 35 dB, with the normalized Doppler frequency of 0.25. The range-Doppler spectrum of received data is shown in Fig 14, it can be found that the true target is covered by the clutter and the discrete interference is obvious at different Doppler frequency. In the verification, the number of spatial bins and Doppler bins are $N_s = 6N$ and $N_d = 6M$, 4 range cell data around the 299th range cell are selected as the training data. The loading factor is set to 10 dB above the noise power level and the threshold is $10^{-3}$ time of the noise power.

Fig. 15 shows the output SINR with respect to the normalized Doppler frequency. It is observed that the proposed method can obtain better SINR compared with the M-FOCUSS method and the SBL method. The proposed R-SBL method achieves almost identical performance as the G-SBL method and the FB-SBL method with much less computations. Afterwards, we depict the range detection performance at target Doppler frequency in Fig. 16. It is evident all sparsity-based STAP methods can obtain desirable detection, and compared with the M-FOCUSS and the SBL methods, the proposed R-SBL method achieves improved range detection performance.

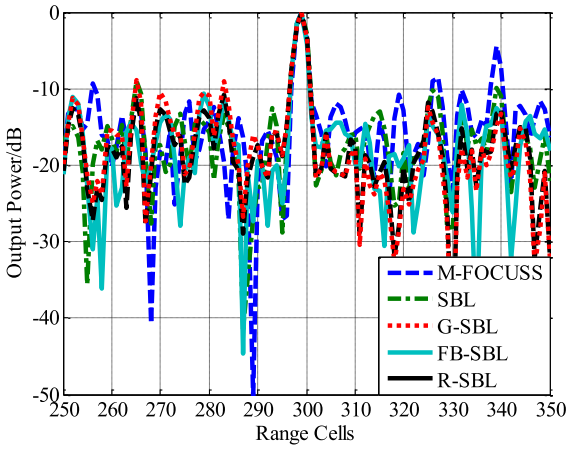


**FIGURE 16.** Range detection performance at target Doppler frequency of M-FOCUSS, SBL, G-SBL, FB-SBL and proposed R-SBL methods based on MCARM data.

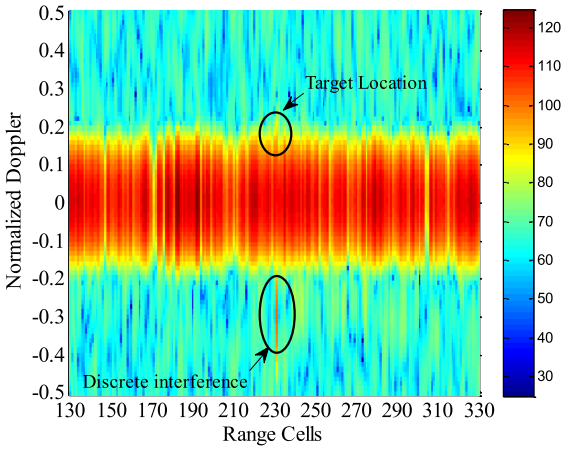


**FIGURE 17.** The range-Doppler spectrum of actual measured airborne radar data.

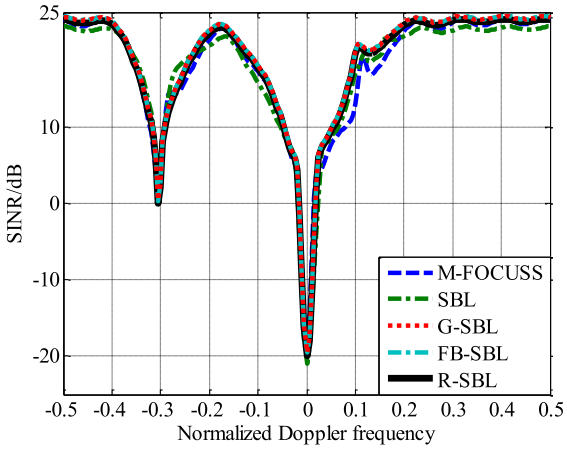


**FIGURE 18.** Output SINRs of M-FOCUSS, SBL, G-SBL, FB-SBL and proposed R-SBL methods based on actual measured airborne radar data.

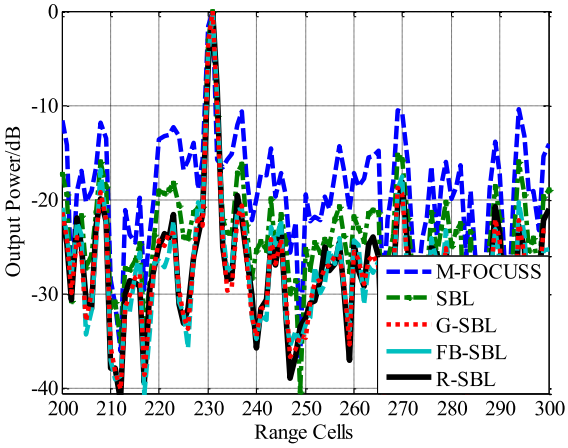


**FIGURE 19.** Range detection performance at target Doppler frequency of M-FOCUSS, SBL, G-SBL and proposed R-SBL methods based on actual measured airborne radar data.

### 2) ACTUAL MEASURED AIRBORNE RADAR DATA

Afterwards, 8 channels and 16 pulses of the actual airborne radar data are utilized. A strong target is located at the 231th range cell with a normalized Doppler frequency of about 0.07 [16]. in the verification, we use $N_s = 6N$ and $N_d = 6M$, and the INR of the discrete interference is 30 dB. The normalized Doppler frequency is -0.3. The range-Doppler spectrum of received data is shown in Fig 17, it can also be found that the true target is covered by the clutter and the discrete interference is obvious at different Doppler frequency. 4 range cell data around the 231st range cell are used as the training data. The loading factor is 10 dB above the noise level and the threshold is set to about $10^{-3}$ time of the noise level.

From the output SINR results shown in Fig. 18, it is seen that the proposed R-SBL method achieves better performance especially in the main-lobe region compared with the M-FOCUSS and the SBL methods. Fig. 19 compared the range detection performance at target Doppler frequency, which is similar to that obtained from the simulated data example, i.e., the proposed method offers better range detection performance. It thus verifies that the proposed R-SBL method gives improved performance in a practical clutter environment.

## VII. CONCLUSION

In this paper, a space-time discrete interference suppression method based on robust SBL has been proposed by investigating the sparse property of spatial-temporal clutter spectrum. In proposed method, the spectral distribution is estimated based on the MAP principle and the mismatch of overcomplete dictionary is calibrated by calculating the error matrix. Due to the robust clutter spectrum estimation, the proposed method can simultaneously suppress the discrete interference and homogeneous clutter effectively. The proposed method can improve the detection performance with less computational complexity compared with existing STAP methods. The effectiveness of the proposed method was verified based on the simulated and actual airborne phased array radar data.

## REFERENCES


[1] J. R. Guerci, *Space-Time Adaptive Processing for Radar*. Norwood, MA, USA: Artech House, 2003.

[2] J. Ward, "Space-time adaptive processing for airborne radar," MIT Lincoln Lab., Lexington, MA, USA, Tech. Rep. 1015, Dec. 1994.

[3] W. L. Melvin, "Space-time adaptive radar performance in heterogeneous clutter," *IEEE Trans. Aerosp. Electron. Syst.*, vol. 36, no. 2, pp. 621–633, Apr. 2000.

[4] T. K. Sarkar *et al.*, "A deterministic least-squares approach to space-time adaptive processing (STAP)," *IEEE Trans. Antennas Propag.*, vol. 49, no. 1, pp. 91–103, Jan. 2001.

[5] W. Choi, T. K. Sarkar, H. Wong, and E. L. Mokole, "Adaptive processing using real weights based on a direct data domain least squares approach," *IEEE Trans. Antennas Propag.*, vol. 54, no. 1, pp. 182–191, Jan. 2006.

[6] R. S. Adve, T. B. Hale, and M. C. Wicks, "Practical joint domain localised adaptive processing in homogeneous and nonhomogeneous environments. 2. Nonhomogeneous environments," *IEE Proc. Radar, Sonar Navigat.*, vol. 147, no. 2, pp. 66–74, Apr. 2000.

[7] X. Yang, Y. Sun, Y. Liu, and T. Long, "Hybrid STAP approach of direct data domain algorithm and adaptive localised domain transformation for discrete interference suppression in non-homogeneous clutter," *Electron. Lett.*, vol. 50, no. 23, pp. 1743–1745, Jun. 2014.

[8] Y. Liu, T. Long, and X. Yang, "$D^3$-STMB hybrid STAP algorithm for discrete interference suppression in nonhomogeneous clutter," *IEICE Trans. Commun.*, vol. E94-B, no. 4, pp. 1114–1117, 2011.

[9] J. T. Parker and L. C. Potter, "A Bayesian perspective on sparse regularization for STAP post-processing," in *Proc. IEEE Radar Conf.*, May 2010, pp. 1471–1475.

[10] I. W. Selesnick, S. U. Pillai, K. Y. Li, and B. Himed, "Angle-doppler processing using sparse regularization," in *Proc. IEEE Int. Conf. Acoust. Speech Signal Process.*, Mar. 2010, pp. 2750–2753.

[11] J. A. Tropp, "Just relax: Convex programming methods for identifying sparse signals in noise," *IEEE Trans. Inf. Theory*, vol. 52, no. 3, pp. 1030–1051, Mar. 2006.

[12] W. Weiwei, L. Guisheng, Z. Shengqi, and Z. Jie, "Compressive sensing-based ground moving target indication for dual-channel synthetic aperture radar," *IET Radar, Sonar & Navigat.*, vol. 7, no. 8, pp. 858–866, Oct. 2013.

[13] K. Sun, H. Meng, Y. Wang, and X. Wang, "Direct data domain STAP using sparse representation of clutter spectrum," *Signal Process.*, vol. 91, no. 9, pp. 2222–2236, 2011.

[14] K. Sun, H. Zhang, G. Li, H. Meng, and X. Wang, "A novel STAP algorithm using sparse recovery technique," in *Proc. IEEE Int. Geosci. Remote Sens. Symp.*, Jul. 2009, pp. 336–339.

[15] Z. Yang, X. Li, H. Wang, and L. Nie, "Sparsity-based space-time adaptive processing using complex-valued Homotopy technique for airborne radar," *IET Signal Process.*, vol. 8, no. 5, pp. 552–564, Jul. 2014.

[16] X. Yang, Y. Sun, T. Zeng, and T. Long, "Robust and fast iterative sparse recovery method for space-time adaptive processing," *Sci. China Inf. Sci.*, vol. 59, no. 6, pp. 062308-1–062308-13, 2016.

[17] Y. Sun, X. Yang, T. Long, and T. K. Sarkar, "Robust sparse Bayesian learning STAP method for discrete interference suppression in nonhomogeneous clutter," in *Proc. IEEE Radar Conf. (RadarConf)*, Seattle, WA, USA, May 2017, pp. 1003–1008.

[18] M. Carlin, P. Rocca, G. Oliveri, F. Viani, and A. Massa, "Directions-of-arrival estimation through Bayesian compressive sensing strategies," *IEEE Trans. Antennas Propag.*, vol. 61, no. 7, pp. 3828–3838, Jul. 2013.

[19] S. Qin, Y. D. Zhang, Q. Wu, and M. G. Amin, "DOA estimation of nonparametric spreading spatial spectrum based on Bayesian compressive sensing exploiting intra-task dependency," in *Proc. IEEE Int. Conf. Acoust., Speech Signal Process. (ICASSP)*, Brisbane, QLD, Australia, Apr. 2015, pp. 2399–2403.

[20] L. Poli, G. Oliveri, F. Viani, and A. Massa, "MT–BCS-based microwave imaging approach through minimum-norm current expansion," *IEEE Trans. Antennas Propag.*, vol. 61, no. 9, pp. 4722–4732, Sep. 2013.

[21] Q. Wu, Y. D. Zhang, M. G. Amin, and B. Himed, "Multi-static passive SAR imaging based on Bayesian compressive sensing," *Proc. SPIE Compressive Sens. III*, vol. 9109, May 2014, Art. no. 910902.

[22] G. Oliveri, M. Carlin, and A. Massa, "Complex-weight sparse linear array synthesis by bayesian compressive sampling," *IEEE Trans. Antennas Propag.*, vol. 60, no. 5, pp. 2309–2326, May 2012.

[23] Q. Wu, Y. D. Zhang, M. G. Amin, and B. Himed, "Space–time adaptive processing and motion parameter estimation in multistatic passive radar using sparse Bayesian learning," *IEEE Trans. Geosci. Remote Sens.*, vol. 54, no. 2, pp. 944–957, Feb. 2016.

[24] Y. D. Zhang and B. Himed, "Space-time adaptive processing in bistatic passive radar exploiting complex Bayesian learning," in *Proc. IEEE Radar Conf.* Cincinnati, OH, USA, May 2014, pp. 923–926.

[25] B. D. Rao, K. Engan, S. F. Cotter, J. Palmer, and K. Kreutz-Delgado "Subset selection in noise based on diversity measure minimization," *IEEE Trans. Signal Process.*, vol. 51, no. 3, pp. 760–770, Mar. 2003.

[26] D. P. Wipf and B. D. Rao, "Sparse Bayesian learning for basis selection," *IEEE Trans. Signal Process.*, vol. 52, no. 8, pp. 2153–2164, Aug. 2004.

[27] X. Tan, W. Roberts, J. Li, and P. Stoica, "Sparse learning via iterative minimization with application to MIMO radar imaging," *IEEE Trans. Signal Process.*, vol. 59, no. 3, pp. 1088–1101, Mar. 2011.

[28] M. E. Tipping, "Sparse bayesian learning and the relevance vector machine," *The J. Mach. Learn. Res.*, vol. 1, no. 3, pp. 211–244, 2001.

[29] S. F. Cotter, B. D. Rao, K. Engan, and K. Kreutz-Delgad, "Sparse solutions to linear inverse problems with multiple measurement vectors," *IEEE Trans. Signal Process.*, vol. 53, no. 7, pp. 2477–2488, Jul. 2005.

[30] A. Haimovich, "The eigencanceler: Adaptive radar by eigenanalysis methods," *IEEE Trans. Aerosp. Electron. Syst.*, vol. 32, no. 2, pp. 532–542, Apr. 1996.

[31] D. L. Donoho, M. Elad, and V. N. Temlyakov, "Stable recovery of sparse overcomplete representations in the presence of noise," *IEEE Trans. Inf. Theory*, vol. 52, no. 1, pp. 6–18, Jan. 2006.

[32] E. J. Candès, J. K. Romberg, and T. Tao, "Stable signal recovery from incomplete and inaccurate measurements," *Commun. Pure Appl. Math.*, vol. 59, no. 8, pp. 1207–1223, 2006.

[33] R. Badeau, B. David, and G. Richard, "Fast approximated power iteration subspace tracking," *IEEE Trans. Signal Process.*, vol. 53, no. 8, pp. 2931–2941, Aug. 2005.

[34] Z. Yang, C. Zhang, and L. Xie, "Robustly stable signal recovery in compressed sensing with structured matrix perturbation," *IEEE Trans. Signal Process.*, vol. 60, no. 9, pp. 4658–4671, Sep. 2012.

[35] L. Bai, S. Roy, and M. Rangaswamy, "Compressive radar clutter subspace estimation using dictionary learning," in *Proc. IEEE Radar Conf. (RadarCon)*, Ottawa, ON, Canada, May 2013, pp. 1–6.

[36] B. N. S. Babu, J. A. Torres, and W. L. Melvin, "Processing and evaluation of multichannel airborne radar measurements (MCARM) measured data," in *Proc. IEEE Int. Symp. Phased Array Syst. Tech.*, Boston, MA, USA, Oct. 1996, pp. 395–399.

[37] M. E. Tipping and A. C. Faul, "Fast marginal likelihood maximisation for sparse Bayesian models," in *Proc. 9th Int. Workshop Artif. Intell. Statist.*, C. M. Bishop and B. J. Frey, Eds. Key West, FL, USA, 2003, pp. 3–6.

[38] Z. Zhang and B. D, Rao, "Extension of SBL algorithms for the recovery of block sparse signals with intra-block correlation," *IEEE Trans. Signal Process.*, vol. 61, no. 8, pp. 2009–2015, Apr. 2013.


Authors' photographs and biographies not available at the time of publication.